A Comparative Study of Several Material Models for Prediction of Hyperelastic Properties: Application to Silicone-Rubber and Soft Tissues

P. A. L. S. Martins*, R. M. Natal Jorge* and A. J. M. Ferreira†

* IDMEC/Faculdade de Engenharia da Universidade do Porto, Rua Dr. Roberto Frias, 4200-465 Porto, Portugal

† DEMEGI/Departamento de Engenharia Mecânica e Gestão Industrial da Faculdade de Engenharia da Universidade do Porto, Rua Dr. Roberto Frias, 4200-465 Porto, Portugal

ABSTRACT: The correct modelling of constitutive laws is of critical importance for the analysis of mechanical behaviour of solids and structures. For example, the understanding of soft tissue mechanics, because of the nonlinear behaviour commonly displayed by the mechanical properties of such materials, makes common place the use of hyperelastic constitutive models. Hyperelastic models however, depend on sets of variables that must be obtained experimentally. In this study the authors use a computational/experimental scheme, for the study of the nonlinear mechanical behaviour of biological soft tissues under uniaxial tension. The material constants for seven different hyperelastic material models are obtained via inverse methods. The use of Martins's model to fit experimental data is presented in this paper for the first time. The search for an optimal value for each set of material parameters is performed by a Levenberg–Marquardt algorithm. As a control measure, the process is fully applied to silicone-rubber samples subjected to uniaxial tension tests. The fitting accuracy of the experimental stress–strain relation to the theoretical one, for both soft tissues and silicone-rubber (typically nonlinear) is evaluated. This study intents also to select which material models (or model types), the authors will employ in future works, for the analysis of human soft biological tissues.

KEY WORDS: *hyperelastic properties, soft tissues, uniaxial tests*

Introduction

Experimental measurements of the stress–strain relationship for rubber materials, gave Mooney [1] and Rivlin [2] enough evidence that the linear theory of elasticity, especially Hooke's law, used since the 17th century, was an inadequate approach to access the mechanical properties of such materials. Linear elasticity failure on capturing, the nonlinear mechanical properties of rubber like materials, may be clearly seen on the stress–strain graph curve of a rubber sample subjected to a uniaxial tension test.

In order to study materials with nonlinear mechanical properties, which usually undergo large strains with small applied stresses, a nonlinear version of the classical elasticity theory was developed [3–5]. The nonlinear theory of elasticity, which constitutes the theoretical basis for the study of hyperelastic materials, such as elastomers [4] uses a strain-energy function (Ψ) to describe in energetic terms the mechanical behaviour of this class of materials.

The field of Biomechanics nowadays [6], brings the need of studying the mechanical behaviour of biological materials, since in many ways, people's quality of life may benefit directly from this knowledge [7, 8]. From the works of scientists like Veronda and Westmann [9] and Fung [10], whose pioneering research pave the way for the actual development stage of the biomechanics field, the nonlinear nature of the mechanical properties of some biological soft tissues came to light. This is a common characteristic between some biological materials and elastomers [10]. The application of the nonlinear theory of elasticity to biological soft tissues is therefore a logical path to follow. The aim of this work is to develop and implement a computational strategy for the assessment of nonlinear mechanical properties of materials with nonlinear behaviour, like silicone-rubber, subjected to large strains. This approach is also valid for hydrated biological soft tissues, in special pig muscular tissue, as the authors show in the paper.

The materials (both silicone-rubber and pig muscular tissue) are assumed to be isotropic and incompressible. This assumption is in general valid for rubber-like materials [11], however for the pig muscular tissue it may constitute a simplification of

the problem, as soft tissues are known to present transverse isotropy symmetry [6], and sometimes they are not completely incompressible [12]. Both materials will be modelled using the finite hyperelasticity theory [4].

The authors use an inverse method to fit the hyperelastic material model constants of seven hyperelastic constitutive models:

- Mooney–Rivlin
- Yeoh
- Neo–Hookean
- Ogden
- Humphrey
- Martins
- Veronda–Westmann

An optimisation code was developed to obtain the analytical force–displacement curves. Such analytical results are then compared with experimental results. Three of the seven material models constitute specialised solutions for the study of soft tissues (Humphrey, Martins and Veronda–Westmann). This way, the characterisation of the silicon rubber nonlinear behaviour in a uniaxial tension experiment, is just a starting point for the generalisation of this set of techniques to biological soft tissues. The use of Martins's model [13] to fit experimental data is presented here for the first time.

The paper is organised as follows. In the section 'Material Models' the structure of strain-energy functions is explained. The authors present briefly each material model rewritten in a standard notation, that tries to evidence the difference between the material models.

The section 'Uniaxial Tension Tests for Incompressible Hyperelastic Materials' presents the analytic expressions under the uniaxial tension test conditions for each material model. Two different analytical approaches are used according to the dependencies of each material model.

The numerical techniques employed in this paper have two distinct components, the optimisation algorithm presented in Appendix A, and the error calculations that allow an evaluation of the solutions quality. The later are presented in the section 'Numerical Simulations Results' as well as the numerical results.

The conclusions are presented in the final section.

Material Models

A hyperelastic material model relies upon the definition of the strain-energy function, which assumes different forms according to the material or class of materials considered. This function is obtained from symmetry, thermodynamic and energetic considerations.

If the material is isotropic, the strain-energy functions (Ψ) depend upon the strain invariants

$$\Psi_{\text{isotropic}} = \Psi(I_1, I_2, I_3) \tag{1}$$

where

$$I_1 = \sum_{i=1}^{3} \lambda_i^2$$
$$I_2 = \sum_{i,j=1}^{3} \lambda_i^2 \lambda_j^2, \quad i \neq j \tag{2}$$
$$I_3 = \prod_{i=1}^{3} \lambda_i^2$$

being, λ_1, λ_2 and λ_3, the principal stretches.

If the hyperelastic material is also incompressible ($I_3 = 1$), Equation (1) takes the form

$$\Psi_{\text{I}} = \Psi(I_1, I_2). \tag{3}$$

As strain invariants depend on principal stretches, (λ_1, λ_2, λ_3), strain-energy functions, may also appear as a function of the stretches:

$$\Psi_{\text{I}} = \Psi(\lambda_1, \lambda_2, \lambda_3). \tag{4}$$

In the particular application of hyperelastic theories to the study of soft tissues, this standard approach started to diverge. In order to capture the physics of soft tissues, biomechanics researchers started to build strain-energy functions considering the anisotropic nature of particular soft tissues.

One approach to capture the nature of such materials is to include an anisotropic contribution to the initial isotropic problem. The strain-energy function would take the form:

$$\Psi = \Psi_{\text{isotropic}} + \Psi_{\text{anisotropic}}. \tag{5}$$

An example of a material model that incorporates anisotropy is given in the section 'Martins material model'.

For an extended description on these and other material models, the reader can consult the Refs [3, 4, 10], among others.

Each material model presented in this paper is at least dependent upon one of the following quantities:

- Principal stretches

  $\lambda_1, \lambda_2, \lambda_3$

- Right Cauchy–Green tensor ([**c**]) invariants

  I_1, I_2, I_3

Table 1: Material model dependencies

	Dependencies			
		Cauchy–Green invariants		
Material models	Principal stretches λ	I_1	I_2	Fibre direction $\vec{n}$
Mooney–Rivlin		×	×	
Yeoh		×		
Neo–Hookean		×		
Ogden	×			
Humphrey		×		
Martins	×			×
Veronda–Westmann		×	×	

- Fibre direction

  $\vec{n}$

As the scope of this work is the field of incompressible isotropic materials under simple tension, there are no dependencies on λ_2, λ_3 and I_3. Table 1 summarises the model dependencies.

Mooney–Rivlin material model

The importance of this model is well known, not only for historical reasons, as it was one of the first hyperelastic models, but also because of its high accuracy in predicting the nonlinear behaviour of isotropic rubber-like materials.

The strain-energy function for this material model is often seen in literature in the form

$$\Psi = \frac{\mu_1}{2}(I_1 - 3) - \frac{\mu_2}{2}(I_2 - 3). \tag{6}$$

For our convenience, material parameters μ_1 and $-\mu_2$ will be c_1 and c_2 respectively, so that we may rewrite last expression in the form:

$$\Psi = \sum_{i=1}^{2} c_i(I_i - 3). \tag{7}$$

Yeoh material model

The Yeoh material model for incompressible (rubber-like) materials was presented for the first time in 1990. The strain-energy function that characterises this model depends only on the first strain invariant (I_1):

$$\Psi = \sum_{i=1}^{3} c_i(I_1 - 3)^i. \tag{8}$$

The material constants c_1,c_2 and c_3 are the parameters that we want to fit in our work.

Neo–Hookean material model

As shown by Holzapfel [4], the Neo–Hookean model was established by the study of vulcanised rubber, using a statistical theory. In this approach, vulcanised rubber is seen as a three-dimensional network of long-chain molecules that are connected at a few points:

$$\Psi = c_1(I_1 - 3). \tag{9}$$

The constant c_1 allows us to know the shear modulus by the relation $\mu = 2c_1$.

Ogden material model

This model, due to Ogden's phenomenological theory of elasticity [3], has the general form:

$$\Psi = \sum_{i=1}^{N} \frac{\mu_i}{\alpha_i}(\lambda_1^{\alpha_i} + \lambda_2^{\alpha_i} + \lambda_3^{\alpha_i} - 3). \tag{10}$$

The $N \times 2$ material constants may be represented in our notation by $\mu_i = c_{2i-1}$ and $\alpha_i = c_{2i}$, so (10) takes the form

$$\Psi = \sum_{i=1}^{N} \frac{c_{(2i-1)}}{c_{2i}}(\lambda_1^{c_{2i}} + \lambda_2^{c_{2i}} + \lambda_3^{c_{2i}} - 3). \tag{11}$$

According to Ref. [4], excellent convergence between theoretical and experimental results for rubber are achieved when $N = 3$.

Humphrey material model

This model was proposed by Humphrey and Yin [14] for the study of passive myocardium. The strain-energy function presented by them has the form:

$$\Psi = c(e^Q - 1) \tag{12}$$

where Q is a function of the components of the right Cauchy–Green tensor. For the purpose of our comparative work a particular isotropic form for Q is chosen as:

$$\Psi = c_1(e^{c_2(I_1-3)} - 1) \tag{13}$$

where c_1 and c_2 are the material parameters and I_1 is the first invariant of the Right–Cauchy tensor.

Martins material model

Martins *et al.* [13] proposed this model for the study of skeletal muscles. As mentioned by the authors, this model is a modified form of the incompressible transversely isotropic hyperelastic model proposed by Humphrey and Yin [14].

The uniaxial tension experiment, forces the passive stretching of the muscle fibres ($\lambda_f > 1$), therefore the active component of the strain-energy function (associated with muscle contraction) is not included. The strain-energy function has the form

$$\begin{aligned} \Psi &= \Psi_I + \Psi_{pass} \\ \Psi_I &= c(e^{b(I_1-3)} - 1) \\ \Psi_{pass} &= A(e^{a(\lambda_f-1)^2} - 1) \end{aligned} \tag{14}$$

where Ψ_I is the isotropic strain energy stored in the material and Ψ_{pass} is the strain energy stored in muscle fibres. λ_f is the stretch observed in the fibre direction, which in this case coincides with the applied stretch.

Material constants b and a have no physical dimensions. However c and A have pressure dimensions.

The strain-energy function (14) appears finally in the notation chosen by the authors:

$$\Psi = c_1(e^{c_2(I_1-3)} - 1) + c_3(e^{c_4(\lambda-1)^2} - 1) \tag{15}$$

with $c = c_1$; $b = c_2$; $A = c_3$; $a = c_4$.

Veronda–Westmann's material model

In 1970, Veronda and Westmann presented a new hyperelastic material model [9]. This model is based on uniaxial tests performed upon skin of cats. This model constitutes the base for the recent study of the cirrhotic Human liver [15].

Veronda–Westmann's strain-energy function depends on the invariants I_1, I_2 and I_3 in his general form:

$$\Psi = c_1\left[e^{\alpha(I_1-3)} - 1\right] - c_2(I_2 - 3) + g(I_3). \tag{16}$$

For incompressible materials, $I_3 = 1$, so $g(I_3) = 0$, and it can also be established that $c_2 = c_1(\alpha/2)$, considerations that simplify (16) into

$$\Psi = c_1\left[e^{\alpha(I_1-3)} - 1\right] - c_1\frac{\alpha}{2}(I_2 - 3). \tag{17}$$

In order to make (17) compatible with the notation followed by the authors, the change $\alpha \to c_2$ provides

$$\Psi = c_1\left[e^{c_2(I_1-3)} - 1\right] - \frac{c_1c_2}{2}(I_2 - 3). \tag{18}$$

Uniaxial Tension Tests for Incompressible Hyperelastic Materials

In this work we assume that silicone-rubber has a mechanical behaviour similar to incompressible hyperelastic materials.

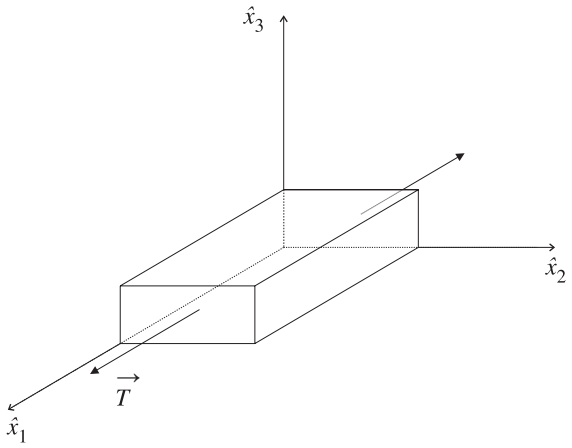

Figure 1: Uniaxial stretching

The general state of a finite deformation is defined by a second-order tensor, commonly known as gradient of deformation

$$F_{aA} = \frac{\partial x_a}{\partial X_A}; \quad a, A = 1, 2, 3. \tag{19}$$

The particular form of $\mathbf{F}$ in the case of hyperelastic materials subjected to an uniaxial tension is

$$[\mathbf{F}] = \begin{bmatrix} \lambda & 0 & 0 \\ 0 & \frac{1}{\sqrt{\lambda}} & 0 \\ 0 & 0 & \frac{1}{\sqrt{\lambda}} \end{bmatrix} \tag{20}$$

assuming that the stress is applied along the $\hat{x}_1$ direction (see Figure 1), taking $\lambda_1 = \lambda$ and noticing that the incompressibility condition

$$J = \prod_{i=1}^{3} \lambda_i = \det(\mathbf{F}) = 1 \tag{21}$$

requires that, $\lambda_2 = \lambda_3 = 1/\sqrt{\lambda}$.

The Right ([**c**]) and Left ([**b**]) Cauchy–Green tensors can be obtained from Equation (20):

$$[\mathbf{c}] = [\mathbf{F}]^T[\mathbf{F}] = \begin{bmatrix} \lambda^2 & 0 & 0 \\ 0 & \lambda^{-1} & 0 \\ 0 & 0 & \lambda^{-1} \end{bmatrix} \tag{22}$$

$$[\mathbf{b}] = [\mathbf{F}][\mathbf{F}]^T = \begin{bmatrix} \lambda^2 & 0 & 0 \\ 0 & \lambda^{-1} & 0 \\ 0 & 0 & \lambda^{-1} \end{bmatrix} \tag{23}$$

and in this particular case are equal.

Now it is possible to define the invariants (2) from the Right Cauchy–Green tensor (22)

$$\begin{aligned} I_1 &= \mathrm{tr}(\mathbf{c}) \\ I_2 &= \frac{1}{2}((\mathrm{tr}(\mathbf{c}))^2 - \mathrm{tr}(\mathbf{c}^2)) \\ I_3 &= \det(\mathbf{c}). \end{aligned} \tag{24}$$

In this particular case they take the form

$$\begin{aligned} I_1 &= \lambda^2 + \frac{2}{\lambda} \\ I_2 &= 2\lambda + \frac{1}{\lambda^2} \\ I_3 &= 1. \end{aligned} \tag{25}$$

Principal Cauchy stresses as a function of stretches

The principal Cauchy stresses for isotropic hyperelastic materials can also be defined as a function of the stretch values. This approach is more convenient for the material models with strain-energy functions that do not depend only on the strain invariants.

One can write with generality that for each principal Cauchy stress:

$$\sigma_i = J^{-1}\lambda_i \frac{\partial \Psi}{\partial \lambda_i}, \quad i = 1, 2, 3. \tag{26}$$

On an isotropic incompressible ($J = 1$) hyperelastic material, one may write each principal Cauchy tension in the following way:

$$\sigma_i = \lambda_i \frac{\partial \Psi}{\partial \lambda_i} + p, \quad i = 1, 2, 3 \tag{27}$$

where p is the hydrostatic pressure which can be determined from the boundary conditions.

For a uniaxial tension experiment, those boundary conditions are:

$$\sigma_2 = \sigma_3 = 0 \tag{28}$$

from which one may finally achieve:

$$\sigma_1 = \lambda_1 \frac{\partial \Psi}{\partial \lambda_1} - \lambda_3 \frac{\partial \Psi}{\partial \lambda_3}. \tag{29}$$

In order to obtain a relation for the uniaxial tension under a particular constitutive model, the strain-energy function for each material model must be rewritten evidencing the stretch dependence.

Cauchy stress as a function of the invariants

Whenever possible use strain-energy functions evidencing a dependence on the invariants, as this approach allows more compact force/stress relations.

According to Holzapfel [4], in the case of a uniaxial tension, the Cauchy stress $\sigma = \sigma_1$ as a function of the strain invariants is

$$\sigma = 2\left(\lambda^2 - \frac{1}{\lambda}\right)\left(\frac{\partial \Psi}{\partial I_1} + \frac{1}{\lambda}\frac{\partial \Psi}{\partial I_2}\right). \tag{30}$$

The other Cauchy stresses vanish since boundary conditions (28) are again valid.

As before, in Equation (30), Ψ must be substituted by the expression corresponding to the material model in study.

Cauchy stresses for each material model

A particular expression is obtained for each material model. To obtain the reaction force from the principal Cauchy stress σ, the sample's cross-section must be found.

In order to compare theoretical and experimental results, the estimated force values must be calculated in the following way.

Let A_f be the final cross-section (A is the original one) so that reaction force is $f = \sigma A_f$.

From the volume conservation we make the following ratio

$$\frac{A}{A_f} = \lambda \tag{31}$$

and the reaction force can be obtained from the initial area

$$f = \frac{A}{\lambda}\sigma. \tag{32}$$

The force value is obtained multiplying the final area with the result of Equation (33).

Mooney–Rivlin model

This material model depends on the invariants I_1 and I_2 (Equation 7), so the Cauchy stress obtained using (30) is

$$\sigma_{\text{Mooney}} = 2\left(\lambda^2 - \frac{1}{\lambda}\right)\left(c_1 + c_2\frac{1}{\lambda}\right). \tag{33}$$

Yeoh model

Using the invariant form of Cauchy stress (30), and the strain-energy function for the Yeoh model (8) we obtain

$$\sigma_{\text{Yeoh}} = 2\left(\lambda^2 - \frac{1}{\lambda}\right)(c_1 + 2c_2(I_1 - 3) + 3c_3(I_1 - 3)^2). \tag{34}$$

Neo–Hookean model

This material model (9), also enables the use of expression (30) to obtain the Cauchy stress in compact form as

$$\sigma_{\text{Hookean}} = 2\left(\lambda^2 - \frac{1}{\lambda}\right)c_1. \tag{35}$$

Ogden model

Ogden model depends on stretch values λ_1, λ_2 and λ_3. In the case of isotropic hyperelastic materials subjected to a simple tension, Equation (11) is simplified into

$$\Psi = \sum_{i=1}^{N} \frac{c_{(2i-1)}}{c_{2i}} \left[\lambda^{c_{2i}} + 2\left(\frac{1}{\sqrt{\lambda}}\right)^{c_{2i}} - 3 \right]. \tag{36}$$

The Cauchy stress is obtained via Equation (29)

$$\sigma_1 = \sum_{i=1}^{N} c_{2i-1}(\lambda^{c_{2i}} - \lambda^{-c_{2i}/2}). \tag{37}$$

In this study we use $N = 3$, obtaining the following Cauchy tension expression with six material parameters

$$\sigma_{\text{Ogden}} = c_1(\lambda^{c_2} - 2^{-1+c_2}\lambda^{-c_2/2}) + c_3(\lambda^{c_4} - 2^{-1+c_4}\lambda^{-c_4/2}) + c_5(\lambda^{c_6} - 2^{-1+c_6}\lambda^{-c_6/2}). \tag{38}$$

Here the inherent complexity of using Equation (29) instead of (30) is clearly noticed.

Humphrey model

As this material model (on this particular form) depends only on I_1 (see Equation 13) the invariant flavour of Cauchy stress is used (30)

$$\sigma_{\text{Humphrey}} = 2\left(\lambda^2 - \frac{1}{\lambda}\right) c_1 c_2 \, \mathrm{e}^{c_2(I_1-3)}. \tag{39}$$

Martins model

Although inspired on Humphrey model, this model exhibits an explicit dependence on the fibres stretch.

According with Martins *et al.* [13] the Cauchy stress tensor is given by

$$[\sigma] = \frac{1}{J}\mathrm{dev}\left[2\frac{\partial \Psi_{\mathrm{I}}}{\partial I_1}[\mathbf{b}] + \frac{\partial \Psi_{\text{pass}}}{\partial \lambda}(\vec{n} \otimes \vec{n})\right] + p[\mathbf{I}] \tag{40}$$

where the operators dev(·) and tr(·) are defined by Equations (41) and (42) respectively, i.e.

$$\mathrm{dev}(\cdot) = (\cdot) - \frac{1}{3}\mathrm{tr}(\cdot)[\mathbf{I}] \tag{41}$$

$$\mathrm{tr}(\cdot) = 2\frac{\partial \Psi_{\mathrm{I}}}{\partial I_1}\left(\lambda^2 + \frac{2}{\lambda}\right) + \frac{\partial \Psi_{\text{pass}}}{\partial \lambda}\lambda. \tag{42}$$

Because of the (assumed) orientation of the fibres in the sample, and the uniaxial tension conditions, $\mathrm{dev}(\cdot)_{22} = \mathrm{dev}(\cdot)_{33}$, so that the components of dev(·) are:

$$\mathrm{dev}(\cdot)_{11} = \frac{4}{3}\frac{\partial \Psi_{\mathrm{I}}}{\partial I_1}\left(\lambda^2 - \frac{1}{\lambda}\right) + \frac{2}{3}\frac{\partial \Psi_{\text{pass}}}{\partial \lambda}\lambda \tag{43}$$

$$\mathrm{dev}(\cdot)_{22} = \frac{2}{3}\frac{\partial \Psi_{\mathrm{I}}}{\partial I_1}\left(\frac{1}{\lambda} - \lambda^2\right) - \frac{1}{3}\frac{\partial \Psi_{\text{pass}}}{\partial \lambda}\lambda = \mathrm{dev}(\cdot)_{33}. \tag{44}$$

From Equation (40) the Cauchy tension in direction 1 is extracted:

$$\sigma_1 = \mathrm{dev}(\cdot)_{11} + p. \tag{45}$$

To find the value of parameter p, the boundary condition imposed upon σ_3 (46) is solved in order to p:

$$\sigma_3 = 0 = \mathrm{dev}(\cdot)_{33} + p \tag{46}$$

where the result

$$p = \frac{2}{3}\frac{\partial \Psi_{\mathrm{I}}}{\partial I_1}\left(\lambda^2 - \frac{1}{\lambda}\right) + \frac{1}{3}\frac{\partial \Psi_{\text{pass}}}{\partial \lambda}\lambda \tag{47}$$

substituted in (45) finally gives:

$$\sigma_1 = 2\frac{\partial \Psi_{\mathrm{I}}}{\partial I_1}\left(\lambda^2 - \frac{1}{\lambda}\right) + \frac{\partial \Psi_{\text{pass}}}{\partial \lambda}\lambda. \tag{48}$$

Following the notation of this paper, Equation (48) is rewritten using the strain-energy function (ψ) from Equation (15) in the section 'Martins material model':

$$\sigma_{\text{Martins}} = 2\left(\lambda^2 - \frac{1}{\lambda}\right) c_1 c_2 \, \mathrm{e}^{c_1(I_1-3)} + 2\lambda(\lambda-1)c_3 c_4 \, \mathrm{e}^{c_3(\lambda-1)^2}. \tag{49}$$

Veronda–Westmann model

This strain-energy function is suited for the application of expression (30). The resultant stress expression, after joining common terms is:

$$\sigma_{\text{Veronda–Westmann}} = 2\left(\lambda^2 - \frac{1}{\lambda}\right) c_1 c_2 \left(\mathrm{e}^{c_2(I_1-3)} - \frac{1}{2\lambda}\right). \tag{50}$$

Numerical Simulations Results

The silicone-rubber is a hyperelastic material which exhibits elastic behaviour for a high degree of deformation, but showing strong nonlinear properties.

Figure 2 shows the geometry of silicone-rubber samples, according to the standard DIN 53504:1994.

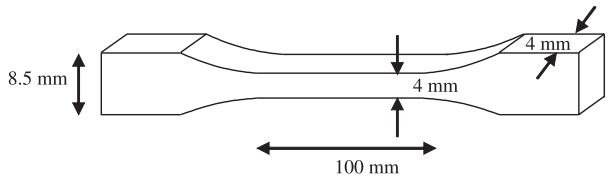

Figure 2: Silicone-rubber sample geometry

The sample preparations and experimental procedure details follow a similar procedure as in Ref. [16].

The simple tension (uniaxial) experiments taken upon pig muscular (soft hydrated) tissue, were performed along the muscle fibre direction. The samples were taken from homogeneous zones of pig muscle where fibres were well oriented, and no visible muscle nerves or other major inhomogeneities were seen. The samples were preserved in a saline bath at 5 °C until testing time in order to avoid dehydration. The geometry of the tissue samples was similar to the geometry of the silicone-rubber samples (Figure 2). For each model, every set of optimal material parameters is obtained with an implementation of the Levenberg–Marquardt (LM) optimisation algorithm in FORTRAN90 [17]. This algorithm is presented in Appendix A.

The graphical treatment of data was made with MATLAB®.

Comparison of seven hyperelastic methods

Hyperelastic material models are more suited to explain the nonlinear elastic behaviour of silicone-rubber under the assumptions of material isotropy and incompressibility.

For this purpose, first we compared the stress–stretch experimental results and the material models predictions obtained by the optimised material parameters. This procedure was also applied to the soft tissue experimental data. Table 2 displays the input parameters and results of each optimisation process.

As seen in Figure 3, the bulk of the studied set of models can capture the general behaviour of the stress–stretch curves for the silicone-rubber. We can draw the same conclusion about soft tissues, observing Figure 4. However, it is clearly seen that the Neo–Hookean material constitutive law is insufficient to capture the nonlinear mechanical behaviour of both materials.

The overall quality of each model's numerical predictions is evaluated calculating correlation coefficients between experimental and theoretical force–displacement data (one for each hyperelastic model).

The correlation coefficient for a given set of m experiments can be given by [18]

$$C.C._{\text{model}} = \frac{\sum_{i=1}^{m}(f_i - \overline{f})_{\text{t}}(f_i - \overline{f})_{\text{e}}}{\sqrt{\sum_{i=1}^{m}(f_i - \overline{f})_{\text{t}}}\sqrt{\sum_{i=1}^{m}(f_i - \overline{f})_{\text{e}}}} \tag{51}$$

where the subscript $(\cdot)_{\text{e}}$ stands for experimental, $(\cdot)_{\text{t}}$ for theoretical and $\overline{f}$ is the mean value of the force.

Table 2: Optimisation results for each material model ($\varepsilon = 1.0 \times 10^{-10}$)

		Silicone-rubber			Soft tissue		
Material model	Seeds (c_i)	C.C.	Nr. It.	Parameters	C.C.	Nr.It.	Parameters
Mooney–Rivlin	1.0	0.99755	3	0.96496	0.99659	3	0.18582
				−0.95833			−0.20583
Yeoh	1.0	0.99988	3	0.24162	0.99995	4	0.004154
				0.19977			0.050753
				−0.00541			−0.013199
Neo–Hookean	0.001	0.97350	2	0.43631	0.95677	2	0.05440
Ogden	1.0	0.99988	135	−0.48953	0.99841	36	0.005044
				1.30073			5.7255
				0.73743			0.005044
				2.95646			5.7255
				−0.60229			0.005044
				1.35266			5.7255
Humphrey	1.0	0.99826	12	1.04600	0.99458	7	0.009348
				0.26751			1.4939
Martins	1.0	0.99994	7	0.67862	0.99978	79	0.53953
				−0.20444			−0.22162
				0.65608			0.79307
				1.43079			0.43009
Veronda–Westmann	1.0	0.99952	12	2.48446	0.99664	5	0.020987
				0.16860			1.0519

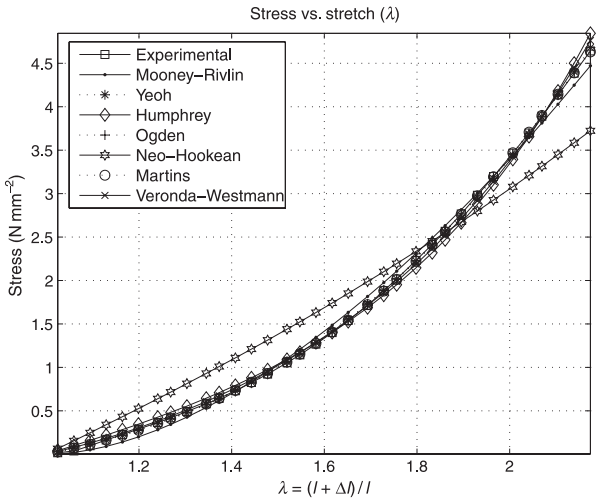

Figure 3: Stress–stretch curves for silicone-rubber

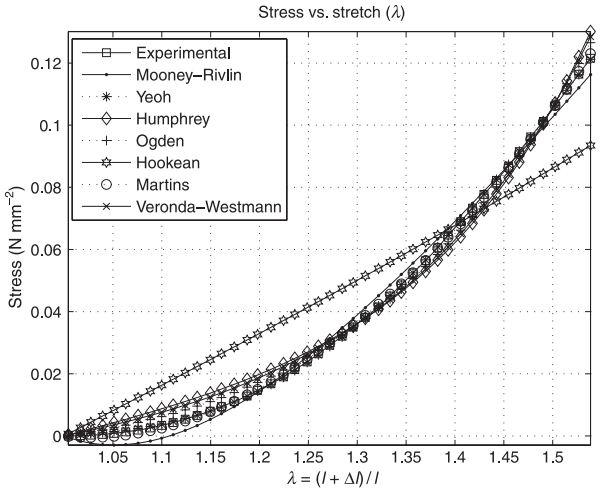

Figure 4: Stress–stretch curves for soft tissues

The correlation coefficients, shown in Table 2, confirm the conclusions made by observation of Figures 3 and 4. It also enables a deeper insight of each model's accuracy on fitting the experimental results. The authors followed the recommendation of Humphrey [18], considering only as valid optimisations those which present C.C. values above 0.90. The graphical representation of this data is presented (for both materials) in Figure 5. It shows that three of the studied hyperelastic material models (Yeoh, Ogden and Martins), allow near exact matches. Another conclusion is that soft tissue's correlation coefficients are smaller (excluding Yeoh's case) than silicone-rubber ones (see Table 2). This fact is justified comparing Figures 3 and 4 by the poorer fitting for small stretches ($\lambda < 1.25$) presented by the latter. The lack of homogeneity, a strong aspect of biological structures, lead us to expect a result of this fashion, where the smoothness of the force–displacement curves is compromised.

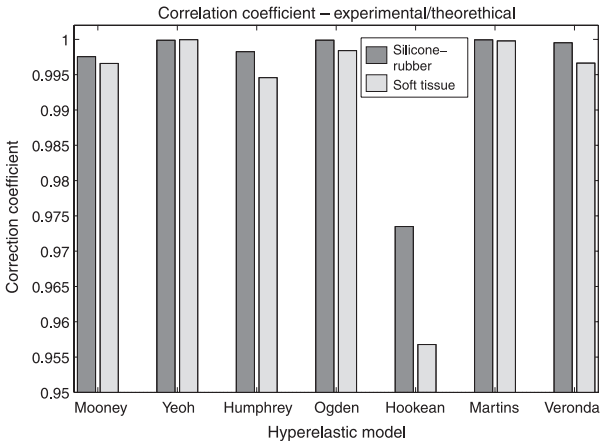

Figure 5: Correlation coefficients

To evaluate more clearly the match between theoretical ($f_t(\lambda)$) and experimental ($f_e(\lambda)$) solutions, we consider silicone-rubber's data, using a normalised error that shows [19] the closeness between results at each stretch level. This error, given in percentage is defined by

$$e_{\%}(\lambda) = \frac{|f_e(\lambda) - f_t(\lambda)|}{f_e(\lambda)} \times 100. \tag{52}$$

In Figure 6 the error analysis for each material model is schematically represented. We can see that for every material model the errors are always higher in the region of small stretches, in agreement with the reports from Ogden *et al.* [20] in their recent work.

A deeper observation of Figure 6 reveals a relation between the number of material parameters (N) in a given model and the number of minima in his error residual curve. In four of the tested material models (Mooney–Rivlin, Humphrey, Veronda–Westmann and Neo–Hookean), this pattern is quite evident due to the error curves smoothness. However, Yeoh, Martins and Ogden models present irregular error curves that are prone to interpretation difficulties. In the case of the Ogden model, in order to gain a better understanding, it was performed a fitting with $N = 4 \times 2$ material parameters. In this model, each pair of material parameters is linked (10), so one would expect that for each pair of material parameters one error minima would appear. The case where ($N = 3 \times 2$) parameters are used (see bottom left graphic of Figure 6) is inconclusive (four minima instead of three) but with $N = 4 \times 2$ constants (see bottom right graphic of Figure 6) are associated the four expected minima.

As for the two remaining models, Yeoh and Martins, we retain any further interpretations for they can always be labelled as questionable.

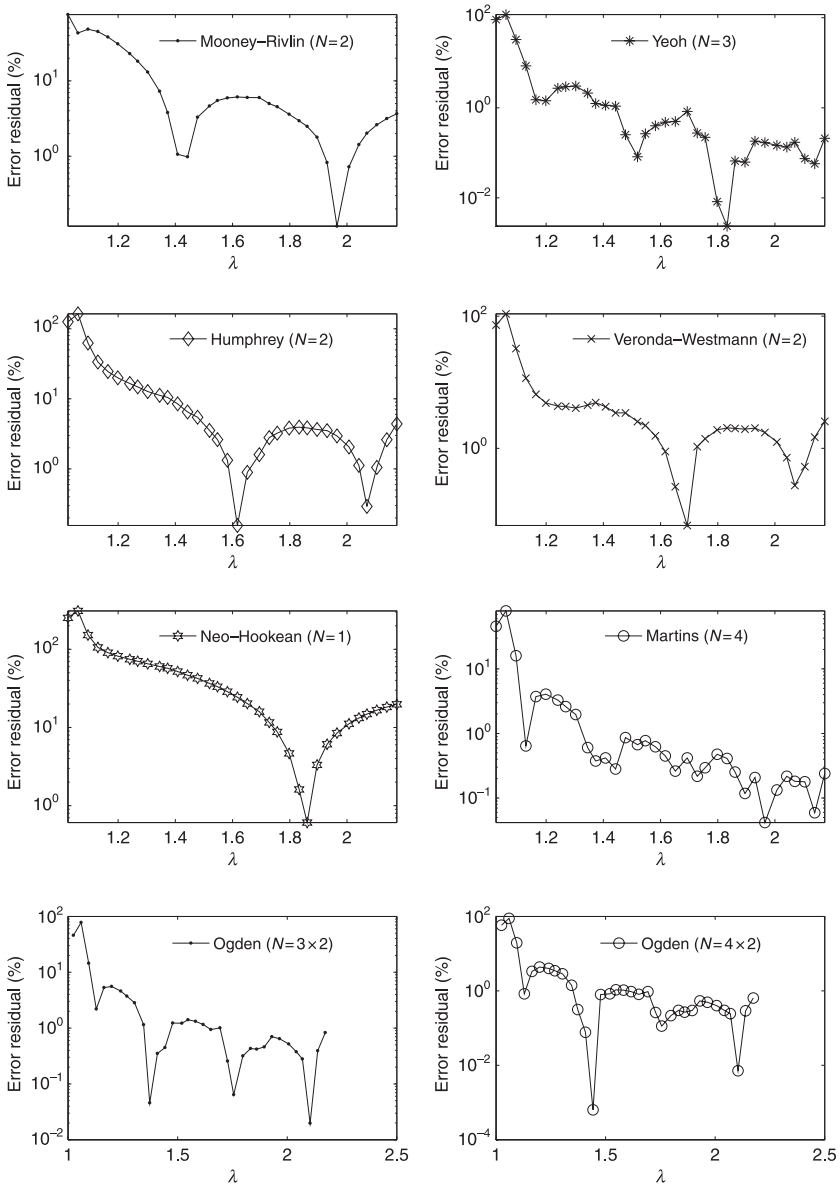

Figure 6: Error residual (%) between experimental and theoretical results for silicone rubber

Optimisation sensibility to Levenberg–Marquardt parameters variation

The LM method uses several parameters, as is explained in Appendix A. On the following sections the authors use silicone-rubber data to understand the influence of two parameters ($\{c_i\}^{\text{seed}}$ and ε) on the method's results.

Influence of ε in LM optimisation

The cost function difference in two consecutive iterations, ε is one of the LM parameters whose influence we tried to assess. From the first optimisation tests, the authors concluded that a good value for ε, in terms of computational cost (iterations) and C.C. is $\varepsilon = 1.0 \times 10^{-10}$. This value was used in all the optimisations presented in Table 2, which were repeated using $\varepsilon = 1.0 \times 10^{-20}$ (with the same seeds).

This procedure showed that the C.C. was immune (up to the fifth decimal place) to the variation of ε. The number of iterations increased for smaller ε values as it would be expected (Table 3).

Worth of notice is the fact that none of the fitted parameter sets suffer any important change with this variation of ε.

Influence of seed sets ($\{c_i\}^{\text{seed}}$) in LM optimisation

The sensitivity analysis concerning the LM seeds ($\{c_i\}^{\text{seed}}$) was performed using the seed sets with equal components. For example if we choose 0.1 as seed value, for the Mooney–Rivlin model, which has two material parameters, $\{c_i\}^{\text{seed}} = \{0.1, 0.1\}$. The range of seeds used was

Table 3: Number of iterations variation with ε

	Number of iterations	
Material model	$\varepsilon = 1.0 \times 10^{-10}$	$\varepsilon = 1.0 \times 10^{-20}$
Mooney–Rivlin	3	6
Yeoh	3	18
Neo–Hookean	2	12
Ogden	135	152
Humphrey	12	21
Martins	7	29
Veronda–Westmann	12	19

$$0.001 \leq \{c_i\}^{\text{seed}} \leq 10\,000.0. \quad (53)$$

In Table 4, the authors present the seed range allowed for each model. With exponential based models (Humphrey, Martins, Veronda–Westmann), and also with the Ogden model, the range of seeds to use is smaller. Seed values either too small or too big, can cause overflow errors despite the double precision arithmetic used on the implementation.

It is clear that the material models whose material parameters appear linearly (Mooney–Rivlin, Yeoh and Neo–Hookean), allow a wider range of initial parameters.

The correlation coefficient (up to the fifth decimal place) for each model and for the range of seeds studied, remain the same of Table 2. The only change noticed (Table 4) was on the number of iterations needed to achieve the stop criteria ($|O(\vec{C}_{k+1}) - O(\vec{C}_k)| \leq \varepsilon$).

Concerning the optimal set of parameters ($\{c_i\}$), there was no important change (up to the third decimal place) for models with a number of material parameters from one to three (Mooney–Rivlin, Yeoh, Neo–Hookean, Humphrey and Veronda–Westmann). However, Ogden and Martins with six and four material parameters respectively, revealed alternative sets of optimal solutions with C.C. changes on the fifth and fourth decimal places. The possibility of obtaining different sets of optimal parameters with the LM algorithm is one of the potential problems that surround the method [21]. According to Ogden *et al.* [20], for models with a small number of material parameters it is expected a small number of optimal solutions. In fact, we found only one set of optimal parameters for models with one, two or three parameters.

Table 4: Seed range for each material model

		Number of iterations	
Material model	Seed range	Left bound	Right bound
Mooney–Rivlin	$0.001 \leq \{c_i\}^{\text{seed}} \leq 10\,000.0$	3	3
Yeoh		3	14
Neo–Hookean		2	3
Ogden	$0.1 \leq \{c_i\}^{\text{seed}} \leq 1.0$	135	152
Humphrey		60 214	12
Martins	$0.01 \leq \{c_i\}^{\text{seed}} \leq 1.0$	100 000	7
Veronda–Westmann	$0.1 \leq \{c_i\}^{\text{seed}} \leq 10.0$	88	389

Conclusions

From the seven analysed material models, six good correlations (>0.99) between experimental and theoretical data are presented. This is valid for the two materials tested, silicone-rubber and soft tissues. In general, the correlations of silicone-rubber were better than the ones of soft tissues. This result makes sense, as biological materials are not as homogeneous as elastomers. The best results were obtained with Yeoh, Ogden and Martins models. Yeoh and Ogden models are generic hyperelastic models, so a suitable description of the material properties is expected to occur for a wide range of materials. The Martins's model [13] is used here for the first time to fit experimental data. It presents very good results for soft tissues as well as for silicone-rubber.

Neo–Hookean model showed the worst performance, unable to capture the nonlinearity of the mechanical properties seen on the two materials.

All the tested material models showed less accuracy on the region of small stretches ($1.0 < \lambda < 1.2$), fact that confirms the observations of Ogden *et al.* [20].

A connection between the number of material parameters of a given material model and the number of minima that his error curve displays was established. As far as the authors' knowledge, this relation is exposed in this work for the first time. Two of the seven models do not display this behaviour clearly.

Exponential-based models (Humphrey, Martins, Veronda–Westmann) and Ogden model were seen to allow narrower intervals of material parameter seeds, when compared with the linear models.

The number of material parameters to fit has influence on the number of potential optimal solutions of the optimisation problem. The authors found only one set of material parameters with models up to three material constants.

This work is the first part of the group's undergoing investigation on the mechanical properties of bio-

logical soft tissues. Issues like anisotropy (or transverse isotropy) and fibre direction, will be addressed on future works. Some of the models tested (Yeoh, Ogden and Martins), allowed very good fittings for both materials, therefore, on the present form or with adequate variations, they will constitute the theoretical basis of further studies.

ACKNOWLEDGEMENTS

The support of Ministério da Ciência e do Ensino superior (FCT and FSE) (Portugal) and the funding by FEDER under grant POCTI/ESP/46835/2002, are gratefully acknowledged.

REFERENCES

1. Mooney, M. (1940) A theory of large elastic deformation. *J. Appl. Phys.* **11**, 582–592.
2. Rivlin, R. S. (1948) Large elastic deformations of isotropic materials. iv: Further developments of the general theory. *Philos. Trans. R. Soc. Lond.* **A241**, 379.
3. Ogden, R. W. (1984) *Non-Linear Elastic Deformations*. Dover Publications Inc., Mineola, NY, USA.
4. Holzapfel, G. A. (2000) *Nonlinear Solid Mechanics*. John Wiley and Sons, New York.
5. Lai, W. M., Rubin, D. and Krempl, E. (1996) *Introduction to Continuum Mechanics*, 3rd edn. Butterworth Heinemann.
6. Humphrey, J. D. (2003) Continuum biomechanics of soft biological tissues. *Proc. Math. Phys. Eng. Sci. (Ser. A)* **459**, 3–46.
7. Azar, F. S., Metaxas, D. N. and Schnall, M. D. (2001) A deformable finite element model of the breast for predicting mechanical deformations under external perturbations. *Acad. Radiol.* **8**, 965–975.
8. Miller, K. (1999) Constitutive model of brain tissue suitable for finite element analysis of surgical procedures. *J. Biomech.* **32**, 531–537.
9. Veronda, D. R. and Westmann, R. A. (1970) Mechanical characterization of skin-finite deformations. *J. Biomech.* **3**, 111–124.
10. Fung, Y. C. (1993) *BIOMECHANICS – Mechanical Properties of Living Tissues*, 2nd edn. Springer-Verlag Inc., New York.
11. Erman, B. and Mark, J. E. (1997) *Structures and Properties of Rubberlike Networks*. Oxford University Press, Oxford.
12. Farshad, M., Barbezat, M., Flüeler, P., Schmidlin, F., Graber, P. and Niederer, P. (1999) Material characterization of the pig kidney in relation with the biomechanical analysis of renal trauma. *J. Biomech.* **32**, 417–425.
13. Martins, J. A. C., Pires, E. B., Salvado, R. and Dinis, P. B. (1998) A numerical model of passive and active behavior of skeletal muscles. *Comput. Methods Appl. Mech. Eng.* **151**, 419–433.
14. Humphrey, J. D. and Yin, F. C. P. (1987) On constitutive relations and finite deformations of passive cardiac tissue: I. A pseudostrain energy function. *ASME J. Biomech. Eng.* **109**, 298–304.
15. Yin, H. M., Sun, L. Z., Wang, G. and Vannier, M. W. (2004) Modeling of elastic modulus evolution of cirrhotic human liver. *IEEE Trans. Biomed. Eng.* **51**, 1854–1856.
16. Areias, P. M. A., Natal Jorge, R. M., Barbosa, J. T., Fernandes, A. A., Mascarenhas, T., Oliveira, M. and Patrício, B. (2003) Experimental and finite element analysis of human skin elasticity. In: *American Society of Mechanical Engineers, Bioengineering Division*, **55**, 303–304.
17. Zhang, Z. (1997) Parameter estimation techniques: a tutorial with application to conic fitting. *Image Vision Computing* **15**, 59–76.
18. Humphrey, J. D. (2002) *Cardiovascular Solid Mechanics*. Springer-Verlag Inc., New York.
19. Meaney, D. F. (2003) Relationship between structural modeling and hyperelastic material behavior: application to CNS white matter. *Biomech. Modeling Mechanobiol.* **1**, 279–293.
20. Ogden, R. W., Saccomandi, G. and Sgura, I. (2004) Fitting hyperelastic models to experimental data. *Comput. Mech.* **34**, 484–502.
21. Kauer, M. (2001) *Inverse Finite Element Characterization of Soft Tissues With Aspiration Experiments*. PhD Thesis, Swiss Federal Institute of Technology, Zürich, Switzerland.

APPENDIX A: ALGORITHM FOR LEVENBERG–MARQUARDT OPTIMISATION

A FORTRAN90 code based on the Levenberg–Marquardt (LM) algorithm was developed. Although several implementations of this algorithm exist on commercial mathematical libraries (e.g. NAG, IMSL), the authors decided to implement their own version of the algorithm.

The aim of this code is to find the optimal value of some set $\{c_1, c_2, \ldots, c_n\}$ of n unknown parameters.

The seven material models considered in this work have the following parameter sets:

- $\{c_1, c_2\}$, set of parameters for the Mooney–Rivlin model
- $\{c_1, c_2, c_3\}$, set of parameters for the Yeoh model
- $\{c_1\}$, set of parameters for the Neo–Hookean model
- $\{c_1, \ldots, c_6\}$, set of parameters for the Ogden model
- $\{c_1, c_2\}$, set of parameters for the Humphrey model
- $\{c_1, \ldots, c_4\}$, set of parameters for the Martins model
- $\{c_1, c_2\}$, set of parameters for the Veronda–Westmann model.

This method is based on the minimisation of a cost function that depends on the analytical model that we are using.

If one needs to fit a generic set of parameters $\{c_1, c_2, \ldots, c_n\}$, simplified in the vectorial form $\vec{C}$ a cost function that compares the squared differences between the analytical model results and the experimental results, must be defined.

A common method to build objective functions $O(\vec{C})$ is given by:

$$O(\vec{C}) = \sum_{i=1}^{m} \omega_i{}^2 [f_i^{\mathrm{an}}(\vec{C}) - f_i^{\mathrm{exp}}]^2 \tag{54}$$

where:

- The summation index m is the number of experimental measurements
- ω_i is the weighting coefficient of the ith measurement.

On the tension experiments considered here, we assume that all measurements are equally 'important', so $\omega_i = 1$, $\forall i : i \in \{1, \ldots, m\}$.

- f_i^{exp} is the force measurement of the ith experimental (*force, displacement*) point
- $f_i^{\mathrm{an}}(\vec{C})$ is the analytic value of force for each material model, according to Equation (32).

The objective function (54) can be expressed using a function $F(\vec{C})$ for each measurement:

$$F_i(\vec{C}) = f_i^{\mathrm{an}}(\vec{C}) - f_i^{\mathrm{exp}} \tag{55}$$

assuming the form:

$$O(\vec{C}) = \sum_{i=1}^{m} F_i(\vec{C})^2. \tag{56}$$

In order to use the LM algorithm, the first and second derivatives of the objective function (56) in order to the hyperelastic model parameters, must be computed

$$\frac{\partial O}{\partial c_k}(\vec{C}) = 2 \sum_{i=1}^{m} F_i \frac{\partial F_i}{\partial c_k} \tag{57}$$

$$\frac{\partial^2 O}{\partial c_k \partial c_l}(\vec{C}) = 2 \sum_{i=1}^{m} \left(\frac{\partial F_i}{\partial c_l} \frac{\partial F_i}{\partial c_k} + F_i \frac{\partial^2 F_i}{\partial c_k \partial c_l} \right), \; k, l = 1, \ldots, n. \tag{58}$$

If $\vec{C}$ is close to the optimal set of parameters (which minimises the value of $O(\vec{C})$), we can assume with little error that $F_i \approx 0$, allowing:

$$\frac{\partial^2 O}{\partial c_k \partial c_l}(\vec{C}) = 2 \sum_{i=1}^{m} \frac{\partial F_i}{\partial c_l} \frac{\partial F_i}{\partial c_k}, \quad k, l = 1, \ldots, n. \tag{59}$$

Writing the set of functions F_i in a vectorial form, $\vec{F} = (F_1, F_2, \ldots, F_m)$, we can analyse the variation of $\vec{F}$ with $\vec{C}$ using a gradient approach:

$$\nabla \vec{F} = \begin{pmatrix} \nabla F \\ \vdots \\ \nabla F_m \end{pmatrix} = \begin{pmatrix} \frac{\partial F_1}{\partial c_1} & \cdots & \frac{\partial F_1}{\partial c_n} \\ \vdots & \cdots & \vdots \\ \frac{\partial F_m}{\partial c_1} & \cdots & \frac{\partial F_m}{\partial c_n} \end{pmatrix}. \tag{60}$$

For simplicity, let $\nabla \vec{F} = [A]$.

Now, in a similar manner, the variation of the objective function is calculated:

$$\nabla O(\vec{C}) = \left(\frac{\partial O}{\partial c_1}, \ldots, \frac{\partial O}{\partial c_n} \right) = \left(2 \sum_{i=1}^{m} F_i \frac{\partial F_i}{\partial c_1}, \ldots, 2 \sum_{i=1}^{m} F_i \frac{\partial F_i}{\partial c_n} \right). \tag{61}$$

From Equation (60) a useful form of Equation (61) is found:

$$\nabla O(\vec{C}) = 2[A]^{\mathrm{T}} \cdot \vec{F}. \tag{62}$$

Considering Equations (59), (60) and (62), the Hessian matrix of the objective function is obtained:

$$\nabla^2 O(\vec{C}) \approx 2[A]^{\mathrm{T}}[A]. \tag{63}$$

Considering an iterative process in which a set of parameters $\vec{C}$ approaches an ideal set of parameters (which minimises the objective function $O(\vec{C})$), is possible to write the following iterative relation:

$$\vec{C}_{k+1} = \vec{C}_k + S_k \vec{d}_k \tag{64}$$

where:

- $\vec{C}_{k+1}$ is the k + 1th set of parameters
- $\vec{C}_k$ is the kth set of parameters
- S_k is the step size
- $\vec{d}_k$ is the displacement direction.

Taking the step size $S_k = 1$ and applying a Newton–Raphson scheme:

$$\vec{C}_{k+1} = \vec{C}_k - [\nabla^2 O]_k^{-1} \cdot (\nabla O)_k \tag{65}$$

Now, rearranging the terms of Equation (65) and considering $\Delta \vec{C}_k = \vec{C}_{k+1} - \vec{C}_k$ we can write the parameter variation expression:

$$\left([A]_k^{\mathrm{T}} [A]_k \right) \cdot \Delta \vec{C}_k = -[A]_k^{\mathrm{T}} \cdot \vec{F}_k. \tag{66}$$

The left side term of Equation (66) is commonly near singular matrix, so in order to overcome this problem, an additional term proportional to the identity matrix $[I]$ is added to the left side term of (66):

$$\left([A]_k^{\mathrm{T}} [A]_k + \lambda_m [I] \right) \cdot \Delta \vec{C}_k = -[A]_k^{\mathrm{T}} \cdot \vec{F}_k, \quad \lambda_m \in R. \tag{67}$$

Equation (67) is the Levenberg–Marquardt method principal operation as we calculate the next set of parameters with

$$\vec{C}_{k+1} = \vec{C}_k + \Delta \vec{C}_k. \tag{68}$$

The complete algorithm (as implemented in FORTRAN90) is:

1. $O(\vec{C}_k)$, $\vec{F}_k \leftarrow \vec{C}_k$, (initial guess $\leftarrow$ $k = 1$)
2. $\nabla\vec{F}_k = [A]_k \leftarrow \vec{C}_k$
3. $[A]_k^{\mathrm{T}}[A]_k + \lambda_m[I] \leftarrow ([A]_k, \lambda_M)$
$[A]_k^{\mathrm{T}} \cdot \vec{F}_k \leftarrow ([A]_k, \vec{F}_k)$
4. $\Delta\vec{C}_k \leftarrow ([A]_k^{\mathrm{T}}[A]_k + \lambda_m[I]) \cdot \Delta\vec{C}_k = -[A]_k^{\mathrm{T}} \cdot \vec{F}_k$
5. $\vec{C}_{k+1} \leftarrow \vec{C}_k + \Delta\vec{C}_k$
6. $O(\vec{C}_{k+1}) \leftarrow \vec{C}_k$
7. if $|O(\vec{C}_{k+1}) - O(\vec{C}_k)| \leq \varepsilon$ then
8. SAVE$\vec{C}_{k+1}$
9. EXIT PROGRAM
10. end if
11. if $O(\vec{C}_{k+1}) \leq O(\vec{C}_k)$ then
12. $\vec{C}_k \leftarrow \vec{C}_{k+1}$
13. $O(\vec{C}_k) \leftarrow O(\vec{C}_{k+1})$
14. $\lambda_M \leftarrow \lambda_M/10$
15. GOTO 2
16. else
17. $\lambda_M \leftarrow 10 \times \lambda_M$
18. GOTO 2
19. end if

Notice that the stop criteria presented here is the difference of the objective function in two consecutive iterations (ε). Other criteria were included, like a maximum number of iterations, but for simplicity, they were omitted in the algorithm presented above.